

## Genetic deletion of *trkB.T1* increases neuromuscular function

Susan G. Dorsey,<sup>1\*</sup> Richard M. Lovering,<sup>2</sup> Cynthia L. Renn,<sup>1</sup> Carmen C. Leitch,<sup>1</sup> Xinyue Liu,<sup>9</sup> Luke J. Tallon,<sup>9</sup> Lisa DeShong Sadzewicz,<sup>9</sup> Abhishek Pratap,<sup>9</sup> Sandra Ott,<sup>9</sup> Naomi Sengamalay,<sup>9</sup> Kristie M. Jones,<sup>9</sup> Colleen Barrick,<sup>7</sup> Gianluca Fulgenzi,<sup>7</sup> Jodi Becker,<sup>7</sup> Kevin Voelker,<sup>3</sup> Robert Talmadge,<sup>4</sup> Brandon K. Harvey,<sup>5</sup> Ryan M. Wyatt,<sup>6</sup> Elizabeth Vernon-Pitts,<sup>6</sup> Chao Zhang,<sup>8</sup> Kevan Shokat,<sup>8</sup> Claire Fraser-Liggett,<sup>9</sup> Rita J. Balice-Gordon,<sup>6</sup> Lino Tessarollo,<sup>7</sup> and Christopher W. Ward<sup>1\*</sup>

University of Maryland Baltimore <sup>1</sup>School of Nursing and <sup>2</sup>School of Medicine, Baltimore, Maryland; <sup>3</sup>Department of Human Nutrition, Foods and Exercise, Virginia Tech, Blacksburg, Virginia; <sup>4</sup>Department of Biological Sciences, California State Polytechnic University, Pomona, California; <sup>5</sup>National Institute of Drug Abuse, National Institutes of Health, Bethesda, Maryland; <sup>6</sup>Department of Neuroscience, University of Pennsylvania School of Medicine, Philadelphia, Pennsylvania; <sup>7</sup>Mouse Cancer Genetics Program, Center for Cancer Research, National Cancer Institute, Frederick, Maryland; <sup>8</sup>Department of Cellular and Molecular Pharmacology, University of California, San Francisco, California; and <sup>9</sup>Institute for Genome Sciences, University of Maryland Baltimore School of Medicine, Baltimore, Maryland

Submitted 12 November 2010; accepted in final form 22 August 2011

**Dorsey SG, Lovering RM, Renn CL, Leitch CC, Liu X, Tallon LJ, Sadzewicz LD, Pratap A, Ott S, Sengamalay N, Jones KM, Barrick C, Fulgenzi G, Becker J, Voelker K, Talmadge R, Harvey BK, Wyatt RM, Vernon-Pitts E, Zhang C, Shokat K, Fraser-Liggett C, Balice-Gordon RJ, Tessarollo L, Ward CW.** Genetic deletion of *trkB.T1* increases neuromuscular function. *Am J Physiol Cell Physiol* 302: C141–C153, 2012. First published August 24, 2011; doi:10.1152/ajpcell.00469.2010.—Neurotrophin-dependent activation of the tyrosine kinase receptor *trkB.FL* modulates neuromuscular synapse maintenance and function; however, it is unclear what role the alternative splice variant, truncated *trkB (trkB.T1)*, may have in the peripheral neuromuscular axis. We examined this question in *trkB.T1* null mice and demonstrate that in vivo neuromuscular performance and nerve-evoked muscle tension are significantly increased. In vitro assays indicated that the gain-in-function in *trkB.T1*<sup>-/-</sup> animals resulted specifically from an increased muscle contractility, and increased electrically evoked calcium release. In the *trkB.T1* null muscle, we identified an increase in Akt activation in resting muscle as well as a significant increase in *trkB.FL* and Akt activation in response to contractile activity. On the basis of these findings, we conclude that the *trkB* signaling pathway might represent a novel target for intervention across diseases characterized by deficits in neuromuscular function.

neurotrophin; neuromuscular junction; calcium; knockout mouse

WITHIN THE NEUROMUSCULAR SYSTEM, the neurotrophins brain-derived neurotrophic factor (BDNF) and NT-4/5 are released by motor neurons and muscle fibers, respectively, both exerting their effects via the cell surface receptor tropomyosin-related kinase B (*trkB*). There are several alternatively spliced isoforms of *trkB*, including a full-length, catalytically active kinase receptor (*trkB.FL*) and several truncated isoforms, with *trkB.T1* being the most abundant. *trkB.T1* receptors bind neurotrophins with the same affinity as *trkB.FL* receptors, but they lack the catalytic intracellular tyrosine kinase domain necessary to transduce signals via classical pathways (50). Several studies have suggested that *trkB.T1* acts in a dominant

negative fashion to decrease signaling through full-length receptors (24–25), while other studies have suggested unique signaling roles for *trkB.T1*, for example, by modulating Ca<sup>2+</sup> signaling mechanisms (63).

BDNF and NT-4 signaling through *trkB.FL* has been suggested to be activity-dependent, involving signals that provide trophic support, modulation of neuromuscular synaptic structure and function (5, 14, 38, 45, 59), and regulation of satellite cell function and muscle regeneration (17). For example, mice lacking NT-4 expression (5), or in which *trkB.FL* signaling was decreased in muscle fibers by overexpression of *trkB.T1*(25) or reduction in *trkB.FL*(38), show impaired neuromuscular synaptic maintenance and/or function. Furthermore, the genetic ablation of BDNF in the muscle resulted in a decrease in the regenerative capacity of muscle following chemical injury (17). While these functions appear to be modulated by the well-described intracellular signaling cascades downstream of *trkB.FL* (12, 35, 61), a role for truncated *trkB.T1* receptors remains unclear.

In this report, we investigate the physiological role of *trkB.T1* in the neuromuscular axis in vivo by examining the functional consequences of the genetic deletion of *trkB.T1*. We show that in vivo assays of neuromuscular performance and nerve-evoked muscle force showed significant enhancements in *trkB.T1*<sup>-/-</sup> compared with *trkB.T1*<sup>+/+</sup> littermates, with in vitro assays ruling out motor neuron and neuromuscular junction (NMJ) synaptic function as an explanation for the neuromuscular phenotype. Isolated muscle and single-myofiber assays in vitro demonstrated that the enhanced muscle contractility was generated from within the muscle fiber, where both an increase in myofiber size as well as an increase in electrically evoked Ca<sup>2+</sup> release were demonstrated. Furthermore, we demonstrate an enhancement of activity-dependent Akt and p70/S6 kinase (*sk6*) phosphorylation in the *trkB.T1*<sup>-/-</sup> muscle, a finding consistent with both the hypertrophy and contractility gain-of-function phenotype. Finally, we demonstrate that *trkB.T1* deletion proffered protection from acute eccentric injury, a finding consistent with recent reports (8, 58) showing that overexpression of constitutively active Akt protected muscle from eccentric injury by upregulating mRNA and proteins involved in cytoskeleton stability and membrane repair. On the basis of these novel findings, we conclude that the *trkB*

\* S. G. Dorsey (e-mail: sdorsey@son.umaryland.edu) and C. W. Ward contributed equally to this work.

Address for reprint requests and other correspondence: C. W. Ward, Univ. of Maryland, Baltimore, School of Nursing, 655 W. Lombard St., Rm. 752, Baltimore, MD, 21201 (e-mail: ward@son.umaryland.edu).

signaling pathway may represent a new opportunity for intervention across diseases that are characterized by deficits in muscle contractility or increased susceptibility to muscle injury.

## MATERIALS AND METHODS

### Animal Models

The Institutional Animal Care and Use Committee of the University of Maryland School of Medicine approved these experiments.

*trkB.T1*. The strategy to target the *trkB.T1*-specific coding exon has been previously described (22). For the current study, we used homozygous and wild-type littermates obtained from heterozygote *trkB.T1* mice backcrossed 14 times into C57BL/6 mice.

*trkB<sup>F616A</sup>*. The *trkB<sup>F616A</sup>* mice were obtained from Dr. David Ginty (Johns Hopkins University, Baltimore, MD). Targeting of the *trkB* locus and the chemical-genetic strategy have been previously described (13). We backcrossed progeny from the F1 hybrid into the C57BL/6 line for 10 generations. To abrogate *trkB.FL* signaling, mice were given 300  $\mu$ g of INMPP1 or an equivalent volume of vehicle intraperitoneally once per day for 4 days. Briefly, INMPP1 was prepared in DMSO as a 100 mM stock. We diluted the stock in sterile 0.9% saline plus 2.5% Tween-20 and calculated volume to administer per body weight of each mouse.

### Gross Neuromuscular Performance

Basal locomotor activity was assessed in a VersaMax Animal Activity Monitor Chamber (Accuscan Instruments, Columbus, OH). Adult male mice (25–30 g), either wild-type or *trkB.T1<sup>-/-</sup>*, were in a 420  $\times$  420  $\times$  310 mm enclosed Plexiglas box equipped with water bottle and food dispenser at the beginning of the dark half of their light-dark cycle. Animals were allowed to move freely with ad libitum access to food and water for 72 h. Motor activity was monitored using infrared beams and measured by the number of beams broken by the animals.

Forepaw grip strength was determined on a commercial rodent grip strength meter (Columbus Instruments). Peak grip strength was assessed in five successive trials separated by 10–15 s by a single rater blinded to genotype. The highest two values were averaged, normalized to body weight, and used as a measure of the peak grip strength.

### In Vivo Neuromuscular Function

Functional performance specific to the peripheral neuromuscular axis was determined in vivo using direct nerve stimulation as previously described in detail (31). Nerve-evoked muscle contractility of the ankle dorsiflexor muscles (i.e., tibialis anterior, or TA, and extensor digitorum longus, or EDL) was assessed in the deeply anesthetized mouse (isoflurane anesthesia) in which the knee was immobilized with a clamp and the foot secured (90° to the tibia) to a 2 cm footplate on a 305B-LR servomotor (Aurora Scientific). The moment arm of the ankle joint was taken as 1 mm (10).

Nerve-evoked isometric muscle contractility was assessed by percutaneous stimulation (0.1-ms sq. wave pulse at >10% threshold voltage) of the common peroneal nerve with a tetanic train of pulses (500-ms pulse train at 150 Hz). A sequence of three successive tetanic pulses (30-s rest interval) was evaluated. The peak response, normalized to either body weight or TA wet weight, was used for analysis.

### Neuromuscular Synaptic Morphology

Mice were deeply anesthetized with pentobarbital sodium (Nembutal) and intracardially perfused with saline followed by 4% paraformaldehyde in Ringer solution, pH = 7.4. Muscles with a segment of nerve (2–3 mm) were carefully excised, postfixed in paraformaldehyde, rinsed, and processed for immunostaining as previously described (25). Postsynaptic acetylcholine receptors (AChRs) were

stained with tetramethylrhodamine isothiocyanate (TRITC)-conjugated  $\alpha$ -bungarotoxin (Calbiochem) followed by labeling of motor nerve terminals and axons with anti-SV2 or -synaptophysin (Developmental Studies Hybridoma Bank) and anti-heavy neurofilament antibodies (SMI-32, Sternberger Monoclonals) as well as anti-S100 $\beta$  to label perisynaptic Schwann cells (54) and the appropriate fluorescently conjugated secondary antibodies (Jackson Immunologicals). After they were coverslipped in anti-fading medium (Vector Laboratories), individual NMJs were imaged using confocal microscopy (Leica TCS system). Single plane projections were constructed from a Z series of 20–40 images. Neuromuscular synaptic area, length, width, and number of discrete postsynaptic AChR regions [as described previously (25)] were determined using interactive software (Metamorph, version 7, Molecular Devices) and analyzed using ANOVA followed by post hoc tests (SigmaStat, version 3.1).

### Analyses of Neuromuscular Synaptic Transmission

*trkB.T1<sup>-/-</sup>* and *+/+* mice were anesthetized by intraperitoneal injection of 0.05 ml of a mixture of 17.4 mg/ml ketamine and 2.6 mg/ml xylazine (Phoenix Pharmaceuticals, St. Joseph, MO), and the soleus muscle and its innervation were dissected under oxygenated (95% O<sub>2</sub>-5% CO<sub>2</sub>) Rees' Ringer (RR) solution. Muscles were pinned in a Sylgard-lined petri dish and superfused with oxygenated RR, and the muscle nerve was placed into a suction electrode.

Physiological analyses were performed as described previously (37). Briefly, nerve-evoked muscle contractions were visualized by stimulating the nerve with 0.1- to 0.2-ms-duration rectangular pulses at 0.5–1 Hz. The stimulus voltage was adjusted from 0.1 to 10 V, and muscle contractions were visually monitored through a dissecting microscope. To determine whether spontaneous and evoked neurotransmitter release is present, skeletal muscle fibers were superfused with u-conotoxin to inhibit muscle fiber activation. Intracellular recordings were performed using glass microelectrodes filled with 3 M KCl (30–570 M $\Omega$  resistance) with all experiments performed at room temperature. Electrical potentials were amplified using an Axoprobe 1A amplifier (Union City, CA), low-pass filtered at 1 kHz, and digitized at 10 kHz using an analog-to-digital converter (DigiData) and interactive software (Axoscope; Molecular Devices). Muscle fiber resting membrane potential was continuously monitored, and only fibers with resting potentials more hyperpolarized than –40 mV and in which the resting potential did not change by >5 mV during the course of the experiment were studied further. Muscle fiber input resistance was calculated as voltage-current after injection of a 100-ms hyperpolarizing current pulse. Mini-end-plate potentials (mEPPs) were recorded for 10–20 min and analyzed using interactive software (Mini Analysis; Synaptosoft, Decatur, GA). To characterize nerve-evoked end-plate potentials (EPPs), the stimulation voltage to the nerve was varied from 0.01 to 2.00 V. Quantal content was determined under conditions of reduced Ca<sup>2+</sup> (1 mM CaCl) and elevated Mg<sup>2+</sup> (10 mM MgCl<sub>2</sub>) using the method of failures (19–20, 37) or expressed as the ratio of mean end-plate potential amplitude/mean mEPP amplitude. The EPP amplitudes were corrected for nonlinear summation (48) using an *f* value of 0.8. The quantal content, i.e., the number of ACh quanta released after a single nerve impulse, was calculated at each NMJ by dividing the mean corrected EPP amplitude by the mean mEPP amplitude (48). Mean, median, and standard deviation were determined for populations of fibers (*n* = 8–12/group; *n* = 4 mice/genotype) in each condition. Significance between parameters was evaluated with conventional statistical methods (*t*-test, ANOVA; SigmaStat version 3.1).

### In Vitro Muscle Contractility

Muscle performance of the EDL or soleus was assessed in vitro using methods described previously (73). In brief, single EDL or soleus muscles were surgically excised with ligatures at each tendon (5-0 silk suture) and mounted in an in vitro bath between a fixed post

and force transducer (Aurora 300B-LR) operated in isometric mode. The muscle was maintained in physiological saline solution (pH 7.6) containing (in mM) 119 NaCl, 5 KCl, 1 MgSO<sub>4</sub>, 5 NaHCO<sub>3</sub>, 1.25 CaCl<sub>2</sub>, 1 KH<sub>2</sub>PO<sub>4</sub>, 10, HEPES, 10 dextrose, and maintained at 30°C under aeration with 95% O<sub>2</sub>-5% CO<sub>2</sub> throughout the experiment. Resting tension and stimulation current were iteratively adjusted for each muscle to obtain optimal twitch force. During a 5-min equilibration, single twitches were elicited at every 30 s with electrical pulses (0.2 ms) via platinum electrodes running parallel to the muscle. Optimal resting tension was determined and isometric tension was evaluated by 250-ms trains of pulses delivered at 1, 10, 20, 40, 60, 80, 100, and 150 Hz. After the experimental protocol, the muscle rested for 5 min at which time muscle length was determined with a digital micrometer and muscle was trimmed proximal to the suture connections, blotted, and weighed. The cross-sectional area (CSA) for each muscle was determined by dividing the mass of the muscle (g) by the product of its length ( $L_0$ , mm) and the density of muscle [1.06 g/cm<sup>3</sup>; (49)] and is expressed as cm<sup>2</sup>. Muscle output was then expressed as isometric tension (N/cm<sup>2</sup>) determined by dividing the tension (N) by the CSA. Statistical comparisons between groups were performed using ANOVA procedures (SigmaStat version 3.1) for tension (force frequency). Significance was set at  $P < 0.05$ .

#### Muscle Fiber Morphology and Fiber Type

Flash frozen (i.e., isopentane  $\sim -40^\circ\text{C}$ ) EDL or soleus muscles ( $n = 4$  each) from each genotype were serially sectioned (8  $\mu\text{m}$ ) perpendicular to the fiber axis using a Microm cryostat and stained immunohistochemically for fast or slow myosin heavy chain (MHC) isoforms using either antifast or antislow MHC monoclonal antibodies (Sigma) (68, 70) and counterstained with TRITC-conjugated wheat germ agglutinin (WGA) to visualize cell membrane boundaries. The sections were then imaged on a confocal fluorescence microscope (Zeiss Radiance 2100). Image analysis routines (ImageJ; National Institutes of Health, Bethesda, MD) were used to measure the CSA of MHCI and -II positive myofibers from a sample of at least 100 individual muscle fibers per muscle.

A detailed examination of MHC composition was conducted in both EDL and soleus muscles from both genotypes using SDS-PAGE for analysis of MHC isoforms as detailed by Talmadge and Roy (69).

#### Myofiber Calcium Signaling

Electrically evoked calcium (Ca<sup>2+</sup>) transients were assayed in single flexor digitorum brevis (FDB) myofibers using methods previously described (9, 11, 15). In brief, FDB muscles were dissected from adult ( $\sim 8$  wk) *trkB.T1*<sup>-/-</sup> ( $n = 4$ ) or *trkB.T1*<sup>+/+</sup> ( $n = 4$ ) mice. Single, intact myofibers were enzymatically isolated (2 mg/ml collagenase Type A), plated on extracellular matrix (Sigma)-coated imaging dishes (Matek), and maintained in DMEM (Invitrogen) supplemented with 0.2% BSA and 100 mM gentamicin (Sigma). Fibers were kept overnight at 37°C in a 5% CO<sub>2</sub> incubator, and experiments were conducted within 12–24 h of plating. Following passive loading of FDB myofibers with the low-affinity Ca<sup>2+</sup> indicator MagFluo-4AM (5  $\mu\text{M}$ ; 45 min), at 20–22°C electrically evoked fluorescent transients (excitation: 488 nm, emission:  $>515$  nm; Ionoptix PMT system; sampled at 1 KHz) were evaluated by either a single 500- $\mu\text{s}$  square pulse or a 200-ms train of pulses, both delivered with field electrodes placed  $\sim 2$  mm apart across the myofiber. Following the normalization of the fluorescence transient to  $\Delta F/F$ , the peak amplitude of the twitch transient was evaluated as the peak Ca<sup>2+</sup> release from the sarcoplasmic reticulum (SR). The decay time constant of the tetanic train of pulses, fit by a monoexponential decay function (OriginPro 7.5), was assayed as the rate of SR Ca<sup>2+</sup> uptake. Following a prolonged train of pulses, most diffusible and nondiffusible Ca<sup>2+</sup> buffers are saturated and the rate of uptake is mostly dependent of sarco(endo)plasmic reticulum Ca<sup>2+</sup>-ATPase (SERCA) uptake back into the SR (11).

#### Eccentric Injury

Adult *trkB.T1*<sup>+/+</sup> and *trkB.T1*<sup>-/-</sup> mice weighing  $24.3 \pm 2.5$  g were anesthetized with isoflurane (2% with oxygen flow rate of 0.5 l/min). The injury model results in a significant and reproducible injury and has been described previously (44, 62). In brief, anesthesia was confirmed by lack of response to a normally painful stimulus (pinching the foot); the left hindlimb was stabilized and the foot was secured onto a footplate. The axis of the footplate was attached to a stepper motor (T8904 NMB Technologies, Chatsworth, CA), a potentiometer to record angular position, and a torque sensor (QWFK-8M, Sensotec, Columbus, OH) to measure torque. The peroneal nerve was stimulated via subcutaneous needle electrodes (Harvard Apparatus 723742, Cambridge, MA), and proper electrode position was determined by a series of isometric twitches. In addition to visual confirmation of isolated dorsiflexion, an increase in twitch torque in response to increasing voltage indicated that opposing plantar flexor muscles were not being simultaneously stimulated. A custom program was used (Labview version 8.5, National Instruments, Austin, TX) to synchronize contractile activation and onset of ankle rotation. Impulses generated by an S48 square pulse stimulator (Grass Instruments, West Warwick, RI) were 0.1 ms in duration and passed through a PSIU6 stimulator isolation unit (Grass Instruments).

To obtain maximal isometric torque measurements before and after injury, the foot was passively positioned at 30° by the stepper motor, which corresponds with the optimal length ( $L_0$ ) of the muscle, and therefore maximal isometric tension ( $P_0$ ) due to the length-tension relationship of skeletal muscle. A maximal tetanic stimulus (250-ms duration) was induced and torque was recorded. To induce injury in the TA muscle, the foot was placed orthogonal to the leg and we superimposed a lengthening contraction onto a maximal isometric contraction. Specifically, a maximal isometric contraction was obtained in the dorsiflexors and after 200 ms, they were lengthened through a 60° arc of motion at 900°/s, well within physiological limits. The majority of torque produced by the dorsiflexors is from the TA (32–33) and we have shown previously that this model results in injury to this muscle (28, 44, 62). The TA remained stimulated throughout lengthening and was injured by performing 20 lengthening (eccentric) contractions, with at least 1 min between each contraction. To ensure that fatigue was not a factor, isometric contractions described above were induced 3 min after the injury protocol.

#### Immunoblot Analysis

Muscle samples were flash frozen in isopentane cooled on dry ice. Muscles were pulverized and homogenized in 10–15 wt/vol of a Tris-buffered saline with 0.1% Tween-20 (TBST) containing 1% Triton X-100, 10% glycerol, and a protease (Miniccomplete Tablet; Roche) and phosphatase (PhosStop Tablets, Roche) tablet. Equal volumes of homogenate were resolved on 4–12% SDS-PAGE and transferred to nitrocellulose or PVDF membranes (Invitrogen). Non-specific binding was blocked using 5% milk or bovine serum albumin in TBST. Membranes were interrogated with primary antibodies directed against Akt, pAkt (Ser473), or phospho-trk (Y490), which were purchased from Cell Signaling Technologies (Beverly, MA). The trkB antibody was purchased from Upstate Biotechnology. Membranes were incubated with primary antibody overnight. After incubation with the appropriate rabbit or mouse secondary antibody (Amersham), we exposed the membrane to enhanced chemiluminescence with SuperSignal West Pico Chemiluminescent Substrate (Pierce, Rockford, IL) to develop immunoblots. Following autoradiography, tools in ImageJ were used to quantitate the density of protein bands on the immunoblots. All blots were stripped using Strongstrip solution (Amersham) and reprobbed with anti-actin (Sigma) to control for differences in protein loading across lanes.

### RNA Extraction

Tibialis anterior muscle was extracted from each genotype ( $n = 3$ ) and flash frozen in isopentane on dry ice. Frozen samples were pulverized and RNA was extracted using standard TRIzol methods. Following extraction, RNA was column-purified (Qiagen) and RNA quality and quantity were assessed via spectrophotometry (Nanodrop).

### Digital Gene Expression Profiling

We utilized Illumina's Digital Gene Expression Tag Profiling Kit to construct the libraries according to the supplied manufacturer protocol. Briefly, we incubated 1  $\mu$ g of total RNA with magnetic oligo(dT) beads to isolate poly-A RNA. While attached to the beads, first- and second-strand cDNA synthesis was accomplished and samples were digested with the *DpnII* restriction enzyme. Next, the GEX *DpnII* adaptor 1 was ligated to the 5'-end of the RNA and a *MmeI* digest was performed to create the 16-bp tag. The fragments were detached from the beads and the GEX adaptor 2 ligation was performed on the 3'-end of the tag. A PCR amplification using primers complementary to the adaptor sequences was performed to selectively enrich the DNA library. The PCR amplicons were gel purified for sequencing and the library was validated.

We conducted 16 cycles of sequencing on the Illumina Genome Analyzer II. To align and annotate the tagged sequences, we downloaded the pregenerated *DpnII* tag set for Mouse Ensembl V52 from the Stowers Institute for Medical Research ([http://research.stowers-institute.org/microarray/tag\\_tables/](http://research.stowers-institute.org/microarray/tag_tables/); Ariel Paulson), stripped out the in silico tag prefix GATC from the sequence data, and generated two separate eland\_tag files from canonical and noncanonical tags. These files were used in Illumina Pipeline ELAND analysis to annotate the data set and quantify the number of reads per gene for each sample. Briefly, the eland\_tag files (canonical and noncanonical) were formatted using the Genome Analyzer Pipeline 1.0 squash genome utility. Next, base calling was conducted by Bustard starting from IPAR1.0 folder using the Phix174 lane as a control. The eland\_tag alignments were conducted using GERALD on the canonical and noncanonical squash genomes, respectively. Results in the format of s\_N\_sequence.txt files were generated for each lane, and summary files were generated using a combination of Linux shell and Perl scripts. Finally, annotations were added to the tag count files and the data were aggregated by genotype.

## RESULTS

### Gross Neuromuscular Performance Is Enhanced in *trkB.T1*<sup>-/-</sup> Mice

As *trkB.T1* is widely expressed in the central nervous system (CNS), peripheral nervous system, and peripheral organs including muscle, the consequences of the genetic deletion of *trkB.T1* were initially assessed by measures of gross motor behavior and neuromuscular performance. We first assessed basal locomotor activity as a measure of the level of spontaneous motor activity. Over a 72-h period, there was no significant difference ( $P > 0.05$ , Student *t*-test) in horizontal activity ( $394,424 \pm 18,302$  vs.  $388,644 \pm 16,355$  beam breaks), vertical activity ( $46,460 \pm 3,484$  vs.  $48,126 \pm 3,050$  beam breaks) or total distance traveled ( $172,489 \pm 1,742$  vs.  $171,377 \pm 9,495$  cm) for *trkB.T1*<sup>-/-</sup> ( $n = 12$ ) vs. wild-type littermate controls ( $n = 12$ ).

Forepaw grip strength, a sensitive assay used to detect dysfunction in several murine models of motor neuron (1, 29, 67) and muscle disease (56), was used as an indirect measure of gross neuromuscular performance. The peak force in each of five successive trials within 2 min was determined and the two

highest values were averaged and normalized to body weight (Fig. 1A). Despite the mean body weights being slightly smaller for the *trkB.T1*<sup>-/-</sup> mice compared with littermate-matched *trkB.T1*<sup>+/+</sup> mice ( $21.51 \pm 0.71$  vs.  $23.90 \pm 0.85$  g), the mean peak tension was  $\sim 15\%$  greater in *trkB.T1*<sup>-/-</sup> ( $4.88 \pm 0.22$  g/body wt;  $n = 12$ ) compared with *trkB.T1*<sup>+/+</sup> littermates ( $4.13 \pm 0.14$  g/body wt;  $n = 11$ ;  $P < 0.05$ , Student's *t*-test).

### *trkB.T1*<sup>-/-</sup> Mice Exhibit Enhanced Peripheral Neuromuscular Function

It is possible that genetic deletion of *trkB.T1* results in an altered central motor activation of neuromuscular function as *trkB.T1* is expressed within the CNS. To eliminate the contribution of a centrally derived motivation or motor unit recruitment component in these mice, neuromuscular performance was further evaluated in vivo in anesthetized mice. The isometric tetanic torque (Fig. 1B) generated by the ankle dorsiflexors (i.e., TA and EDL) secondary to transcutaneous stimulation of the common peroneal nerve was measured (31). The peak nerve-evoked isometric torque, normalized to body weight, was  $\sim 16\%$  greater in *trkB.T1*<sup>-/-</sup> mice compared with wild-type littermates (Fig. 1B,  $93.58 \pm 7.42$  vs.  $110.8 \pm 10.65$  N $\cdot$ mm<sup>-1</sup>·kg<sup>-1</sup>) despite a smaller body weight ( $26.4 \pm 2.1$  vs.

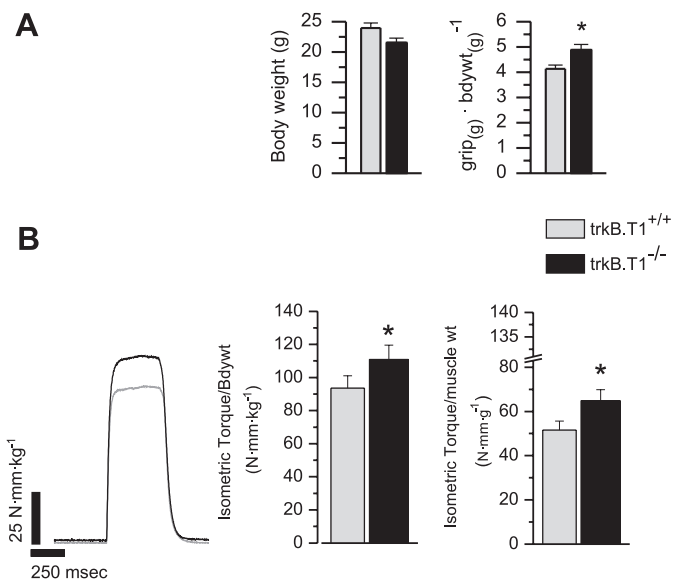


Fig. 1. In vivo neuromuscular performance in *trkB.T1* null mice. A: peak forepaw grip force (right) corrected for body weight (left) was evaluated in *trkB.T1*<sup>+/+</sup> (gray bar,  $4.13 \pm 0.14$ ,  $n = 12$ ) and *trkB.T1*<sup>-/-</sup> (black bar,  $4.88 \pm 0.22$ ,  $n = 12$ ) mice. Peak force (g) was assessed in each of 5 successive trials, and the 2 highest values were averaged and normalized to body weight (grip/bodywt). Bars represent mean peak tension and error bars represent SE.  $*P < 0.05$  by Student's *t*-test. B, left: nerve-evoked muscle force was assessed in ankle dorsiflexors in response to transcutaneous stimulation of the common peroneal nerve. Representative isometric tetanic torque from *trkB.T1*<sup>+/+</sup> (gray) and *trkB.T1*<sup>-/-</sup> (black) is shown. B, right: peak isometric tetanic torque (500-ms train at 100 Hz) was assessed in *trkB.T1*<sup>+/+</sup> vs. *trkB.T1*<sup>-/-</sup> and normalized to either body weight ( $26.4 \pm 2.1$  vs.  $24.2 \pm 1.8$  g,  $n = 6$ /genotype) or wet weight of the excised tibialis anterior muscle ( $47.91 \pm 4.12$  vs.  $41.29 \pm 4.32$  mg,  $n = 6$ /genotype), respectively. Compared with *trkB.T1*<sup>+/+</sup>, *trkB.T1*<sup>-/-</sup> mice exhibited significantly greater tetanic torque when normalized to either body weight ( $93.58 \pm 7.42$  vs.  $110.8 \pm 10.65$  N $\cdot$ mm<sup>-1</sup>·kg<sup>-1</sup>) or muscle weight ( $51.56 \pm 1.09$  vs.  $64.83 \pm 5.06$  N $\cdot$ mm<sup>-1</sup>·g<sup>-1</sup>).  $*P < 0.05$  by ANOVA.

24.2 ± 1.8 g). When normalized to the wet weight of the TA, the *trkB.T1*<sup>-/-</sup> still demonstrated a significant enhancement in muscle torque of ~18% (51.56 ± 1.09 vs. 64.83 ± 5.06 N·mm<sup>-1</sup>·g<sup>-1</sup>) despite the *trkB.T1*<sup>-/-</sup> having a smaller muscle mass (47.91 ± 4.12 vs. 41.29 ± 4.32 mg).

### Muscle Contractility Is Increased in *trkB.T1*<sup>-/-</sup> Mice

To evaluate the muscle specific contribution to the enhancement seen in neuromuscular function assays, we examined muscle-specific contractility in vitro, as we have previously described (18, 73). Individual EDL or soleus muscles were surgically excised, ligatures were placed around each tendon, and muscles were mounted in a bath between a fixed post and a torque sensor (isometric mode) and superfused with oxygenated physiologic saline. Isometric tension was evaluated with 400-ms trains of pulses delivered at 1, 30, 50, 80, 100, and 150 Hz, and the absolute isometric tension produced was normalized to muscle CSA as described (49). In both the EDL and the soleus muscles from *trkB.T1*<sup>-/-</sup> mice, muscle-specific tension was significantly greater at stimulation frequencies above ~30 Hz compared with muscles from wild-type littermates (Fig. 2). At maximal activation (150 Hz), the EDL and soleus muscles from *trkB.T1*<sup>-/-</sup> mice exhibited a 30.1% and 21.2% increase in isometric force. This increase in force was observed without an alteration in the relative position of the force-frequency curve (relationship not shown) or significant alterations in the kinetics of the force transients (Supplemental Table S1; Supplemental Material for this article is available on the Journal website), a result suggestive of a lack of fiber type alteration across genotypes.

### Muscle Fiber Type and Size in *trkB.T1*<sup>-/-</sup> Mice

In our first two experiments we report increases in grip strength and nerve-evoked muscle force in *trkB.T1*<sup>-/-</sup> animals that have the same or slightly smaller body weights than littermate *trkB.T1*<sup>+/+</sup> animals (Fig. 1). Previous reports have

identified neurotrophins as being involved in the maintenance of muscle mass and fiber type following denervation (23, 51, 66). Because an increase in muscle-specific force was observed with nerve-evoked as well as direct muscle stimulation, we asked whether the absence of *trkB.T1* produced an alteration in muscle fiber type and/or size, which might underlie the increase in muscle specific contractility.

Myofiber CSA was assayed in cryosections taken from the mid-belly of soleus and EDL muscles and stained with WGA-conjugated Texas-Red to define fiber boundaries. Figure 3A displays normalized population histograms of fiber sizes within EDL and soleus muscles between genotypes. Across both EDL and soleus muscle groups, myofibers from *trkB.T1*<sup>-/-</sup> mice revealed a larger CSA than *trkB.T1*<sup>+/+</sup> as evidenced by a rightward shifted distribution of fiber sizes (Table 1).

Experiments in which MHC isoforms were electrophoretically separated (Fig. 3B) revealed that MHC type I as well as the MHC type II isoform expression was not significantly different between EDL or soleus muscles across genotypes (Table 2). Taken together, we conclude that *trkB.T1*<sup>-/-</sup> muscles exhibit mild myofiber hypertrophy without any detectable change in MHC fiber type.

### Electrically Evoked Ca<sup>2+</sup> Release Is Greater in *trkB.T1*<sup>-/-</sup> Myofibers

Given that muscle contractility was increased without a significant change in fiber type, we explored other possible explanations for the increase in muscle contractility. As Ca<sup>2+</sup> release from the SR is a positive predictor of myofiber contractile force (6), we next asked whether alterations in myofiber Ca<sup>2+</sup> handling, specifically Ca<sup>2+</sup> release and uptake from the SR, contributed to the increase in muscle contractility seen in muscles from *trkB.T1*<sup>-/-</sup> mice. Electrically evoked SR-dependent Ca<sup>2+</sup> release was assayed in single enzymatically dissociated FDB skeletal myofibers from *trkB.T1*<sup>-/-</sup> mice and wild-type littermates (Fig. 4A). Myofibers loaded with the

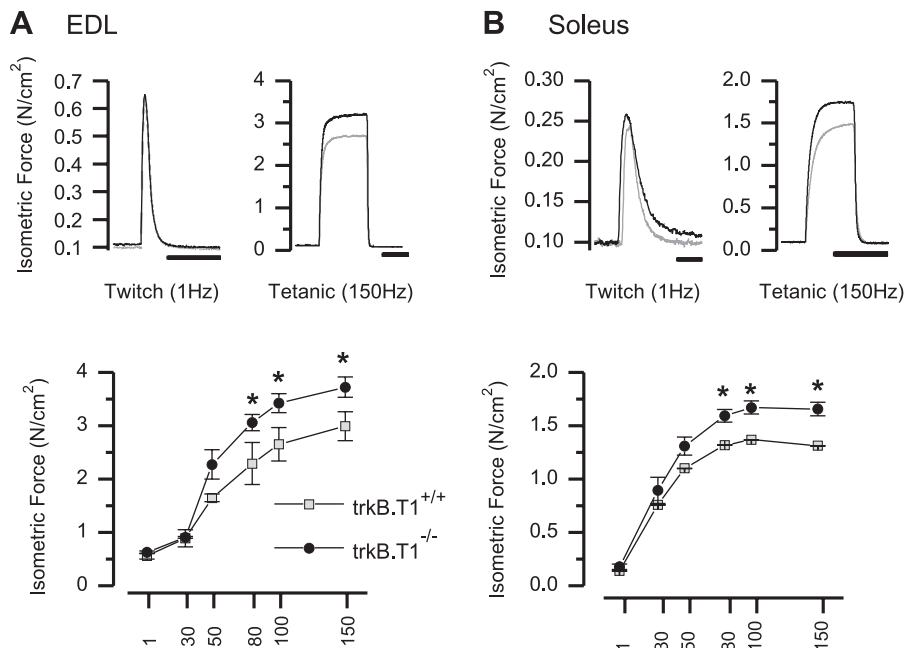


Fig. 2. In vitro contractility of single extensor digitorum longus (EDL) or soleus muscles. EDL and soleus muscles from *trkB.T1*<sup>+/+</sup> and *trkB.T1*<sup>-/-</sup> mice (body weight, 39.14 ± 1.4 vs. 34.24 ± 1.5, respectively) were maintained in physiological saline solution, and isometric tension was evaluated with 1-s trains of pulses delivered at 1, 30, 50, 80, 100, and 150 Hz. *A* and *B*, top: representative twitch and tetanic transients in *trkB.T1*<sup>+/+</sup> (gray) and *trkB.T1*<sup>-/-</sup> mice (black). *A* and *B*, bottom: force (N/cm<sup>2</sup>) vs. stimulation frequency relationship of *trkB.T1*<sup>+/+</sup> (gray, *n* = 5) and *trkB.T1*<sup>-/-</sup> (black, *n* = 6) mice is shown for EDL (muscle weight, 12.54 ± 1.53 vs. 11.40 ± 1.24 mg; *n* = 6) and soleus muscle (muscle weight, 11.83 ± 2.33 vs. 8.25 ± 0.66 mg; *n* = 6). Symbols represent mean force per frequency, with whiskers representing SE. \**P* < 0.05 by ANOVA.

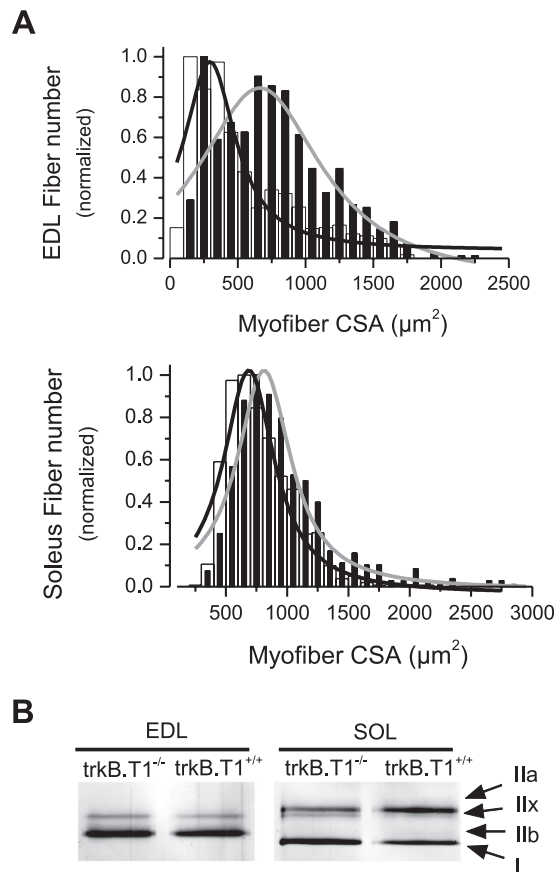


Fig. 3. Muscle fiber phenotype. *A*: histograms of myofiber cross-sectional area (CSA) calculated in all whole fibers. Image analysis was performed in ImageJ using wheat germ agglutinin (WGA)-conjugated Fluorophore to identify the myofiber boundaries. The histogram was fit with a Lorentz function to visualize the data trends in both *trkB.T1*<sup>+/+</sup> (open bar; gray fit) and *trkB.T1*<sup>-/-</sup> (black bar; black fit) muscles. *B*: representative SDS-PAGE gel of electrophoretically separated myosin heavy chain isoforms in EDL and soleus (SOL) muscles across genotypes.

low-affinity fluorescent Ca<sup>2+</sup> indicator MagFluo-4AM (11) were evaluated with either a single action potential (500  $\mu$ s square pulse; Fig. 4*B*) or trains of action potentials delivered at 100 Hz for 200 ms (Fig. 4*C*) through field electrodes placed  $\sim$ 2 mm apart across the myofiber.

The peak amplitude of the fluorescent transient generated by single action potential stimulation was measured as an indicator of the magnitude of Ca<sup>2+</sup> release. Ca<sup>2+</sup> release was significantly greater in *trkB.T1*<sup>-/-</sup> mice ( $0.32 \pm 0.02 \Delta F/F$ ;  $n = 24$ ) compared with wild-type littermates ( $0.25 \pm 0.02 \Delta F/F$ ;  $n = 14$ ; Fig. 4*D*). The decay phase of the Ca<sup>2+</sup> transient after a tetanic train of pulses was assessed as the rate of Ca<sup>2+</sup> uptake back into the SR after release. Following a prolonged stimulus

train, most diffusible (e.g., Ca<sup>2+</sup> dye, parvalbumin) and non-diffusible (e.g., troponin C) Ca<sup>2+</sup> buffers are saturated, and the rate of SR Ca<sup>2+</sup> sequestration is mostly dependent on SERCA activity. Neither the decay time constant after trains of action potentials (the tetanic transient;  $34.16 \pm 4.32$  compared with  $33.26 \pm 3.18$  ms) nor after single action potentials (the twitch transient;  $11.73 \pm 0.74$  ms compared with  $12.31 \pm 1.01$  ms) was different between genotypes. These results indicate that, despite the increase in SR release, the kinetics of Ca<sup>2+</sup> sequestration by SERCA are not affected by the absence of *trkB.T1* expression in muscle fibers.

#### Neuromuscular Junction Morphology Is Mildly Affected in *trkB.T1* Null Mice

Because reducing *trkB.FL* activity in skeletal muscle fibers results in disassembly of postsynaptic AChR clusters and thus NMJs (25), we asked whether neuromuscular junction morphology was altered in the soleus and EDL muscles of *trkB.T1*<sup>-/-</sup> mice compared with *trkB.T1*<sup>+/+</sup> littermates. Motor axons and presynaptic nerve terminals were visualized using antibodies against neurofilaments and the synaptic vesicle protein SV2; perisynaptic Schwann cells were visualized using antibodies against S-100 $\beta$ , and postsynaptic AChR clusters were visualized with fluorescent  $\alpha$ -bungarotoxin as previously described (25). Overall patterns of neuromuscular innervation in the soleus and EDL muscle, specifically that each muscle fiber was innervated at a single end-plate site, were similar between genotypes (Fig. 5*A*). In both muscles, however, a significant increase in the area of postsynaptic AChR clusters was observed in *trkB.T1*<sup>-/-</sup> mice compared with wild-type littermates (Fig. 5, *B* and *C*). This result indicates that NMJ size is modestly increased in *trkB.T1*<sup>-/-</sup> mice, a result not unexpected considering that postsynaptic AChR area scales with increases in myofiber CSA (2).

#### Neuromuscular Synaptic Transmission Is Similar Between *trkB.T1* Null and Wild-Type Mice

Since NMJ size was modestly increased in the *trkB.T1*<sup>-/-</sup> muscles, we then addressed the possibility that enhancements in synaptic transmission contributed to the increased neuromuscular performance in *trkB.T1*<sup>-/-</sup> mice compared with *trkB.T1*<sup>+/+</sup> littermates. Differential expression of *trkB* isoforms has been shown to modulate synaptic transmission (21–22, 40). The soleus muscle was dissected from *trkB.T1*<sup>-/-</sup> and <sup>+/+</sup> mice. Nerve-evoked EPPs and spontaneous mEPPs were analyzed after intracellular recording as previously described (37, 75) (Table 3). Neither mEPP amplitude nor frequency was significantly different between genotypes. Similarly, EPP amplitude, rise time, and quantal content were similar between genotypes. Lastly, measurements of paired

Table 1. Myofiber cross-sectional area in soleus and EDL muscles from *trkB.T1*<sup>+/+</sup> ( $n = 5$ ) and *trkB.T1*<sup>-/-</sup> ( $n = 5$ ) mice

	EDL		Soleus	
	<i>trkB.T1</i> <sup>+/+</sup>	<i>trkB.T1</i> <sup>-/-</sup>	<i>trkB.T1</i> <sup>+/+</sup>	<i>trkB.T1</i> <sup>-/-</sup>
CSA, cm <sup>2</sup>	$1,118.23 \pm 32.44^*$	$1,526.10 \pm 30.19$	$786.43 \pm 8.91^*$	$961.57 \pm 14.90$
$n_{\text{fibers}}$	1,359	711	957	738

Values are means  $\pm$  SE. EDL, extensor digitorum longus; CSA, cross-sectional area. Muscles were the contralateral muscles used for in vitro contractility experiments; therefore the weights stated in Fig. 2 are representative. \* $P < 0.05$ , *trkB.T1*<sup>+/+</sup> vs. *trkB.T1*<sup>-/-</sup>.

Table 2. Myosin heavy chain isotype percentage in soleus and EDL muscles from *trkB.T1*<sup>+/+</sup> (n = 5) and *trkB.T1*<sup>-/-</sup> (n = 5) mice as identified in silver-stained PAGE gels

	EDL		Soleus	
	<i>trkB.T1</i> <sup>+/+</sup>	<i>trkB.T1</i> <sup>-/-</sup>	<i>trkB.T1</i> <sup>+/+</sup>	<i>trkB.T1</i> <sup>-/-</sup>
I	–	–	31.56 ± 4.04	41.9 ± 4.21
IIa	4.9 ± 3.4	3.9 ± 2.3	51.28 ± 5.79	42.17 ± 3.55
IIx	19.8 ± 1.9	17.5 ± 1.3	13.08 ± 2.06	15.25 ± 2.81
IIb	75.3 ± 4.5	78.6 ± 1.9	4.08 ± 3.08	0.68 ± 0.75
n <sub>muscles</sub>	5	6	5	5

Values are means ± SE.

pulse facilitation revealed no difference between genotypes. These results demonstrate that *trkB.T1* does not modulate spontaneous or nerve-evoked neurotransmitter release at neuromuscular junctions.

#### *trkB.T1*<sup>-/-</sup> Muscle Exhibits a Gain in Activity-Induced Akt and p70/sk6 Signaling

As neurotrophin ligand is released in an activity-dependent manner (5, 14, 45, 47, 59), we sought to test whether *trkB.FL*-dependent signaling pathways were differentially activated in *trkB.T1*<sup>-/-</sup> vs. *trkB.T1*<sup>+/+</sup> littermate mice. It is well established that Akt-dependent phosphorylation is downstream of the *trkB.FL* signaling cascade (30, 35, 41). Furthermore, our recent work in *trkB.T1*<sup>-/-</sup> neurons indicates that *trkB.T1* differentially regulates neurotrophin-dependent *trkB.FL* signaling through Akt over ERK (22). In striated muscle, Akt-dependent signaling pathways play a critical role in promoting the transcriptional program associated with muscle hypertrophy as well as increasing muscle contractility (16, 46, 57, 64). Therefore we assayed Akt content as well as basal and activity-

dependent Akt phosphorylation (pAkt) as a potential mechanism for the phenotypes we identified in the *trkB.T1*<sup>-/-</sup>.

Akt and downstream p70/sk6 signaling was assayed in muscle harvested from deeply anesthetized *trkB.T1*<sup>-/-</sup> and *trkB.T1*<sup>+/+</sup> littermate mice in which one hindlimb was stimulated through the peroneal nerve (200-ms train of 50-Hz pulses delivered at 0.25 Hz for 5 min) to exercise the dorsiflexor muscles (i.e., TA and EDL) with isometric contractions. The unstimulated limb served as a within animal control. In the unstimulated TA muscle, Akt content was not different between genotypes (Fig. 6B); however, basal pAkt (Fig. 6C) was increased in the unexercised *trkB.T1*<sup>-/-</sup> muscle. In the exercised TA muscles (Fig. 6D), pAkt increased by approximately twofold in *trkB.T1*<sup>+/+</sup> while *trkB.T1*<sup>-/-</sup> mice exhibited an approximately threefold increase in pAkt, indicating an activity-dependent gain in pAkt activation in the *trkB.T1*<sup>-/-</sup> muscles.

To directly assess the contribution of *trkB.FL* to the activity-dependent increase in Akt phosphorylation, we conducted our in vivo stimulation paradigm in mice genetically engineered with a single-point mutation in the *trkB.FL* protein (F616A) which enables small-molecule (1NMPP1) inhibition of *trkB.FL* signaling (13). Mice homozygous for the mutated allele were intraperitoneally injected daily for 4 days with 300 µg of 1NMPP1 with experiments performed 1 h after the final intraperitoneal injection. Neither basal level of Akt protein or basal pAkt/Akt was different between *trkB*<sup>F616A</sup><sup>-/-</sup> and *trkB.T1*<sup>+/+</sup> (data not shown). Following the 5-min exercise bout, the pAkt/Akt ratio was examined. Figure 6E displays pAkt/Akt postexercise results in the *trkB*<sup>F616A</sup><sup>-/-</sup> mice without (open bar) or with (hatched bar) small-molecule inhibition of *trkB.FL* signaling. The *trkB*<sup>F616A</sup><sup>-/-</sup> muscles displayed an approximate 0.76-fold increase in pAkt with stimulation, a similar fold increase compared with *trkB.T1*<sup>+/+</sup>. Pretreatment with 1NMPP1, the small-molecule inhibitor of *trkB.FL*, signaling resulted in a significant decrease (~25%) in the stimulation-induced pAkt/Akt in the *trkB*<sup>F616A</sup><sup>-/-</sup> compared with the untreated *trkB*<sup>F616A</sup><sup>-/-</sup> (0.76 ± 0.07 vs. 0.57 ± 0.04-fold). These results support a significant role for *trkB.FL* in the activity-dependent increase in Akt phosphorylation.

In striated muscle, activity-dependent activation of Akt is followed by a well-described signaling cascade which includes the activation of sk6 (i.e., p70/sk6). In parallel experiments, we assayed the basal activation and exercise activation of sk6 in *trkB.T1*<sup>+/+</sup> and *trkB.T1*<sup>-/-</sup> mice. Figure 7 reveals that while no differences in sk6 content or basal phosphorylation (Fig. 7B) were seen between genotypes, muscle from *trkB.T1*<sup>-/-</sup> mice exhibited a gain in the activity-dependent activation of sk6

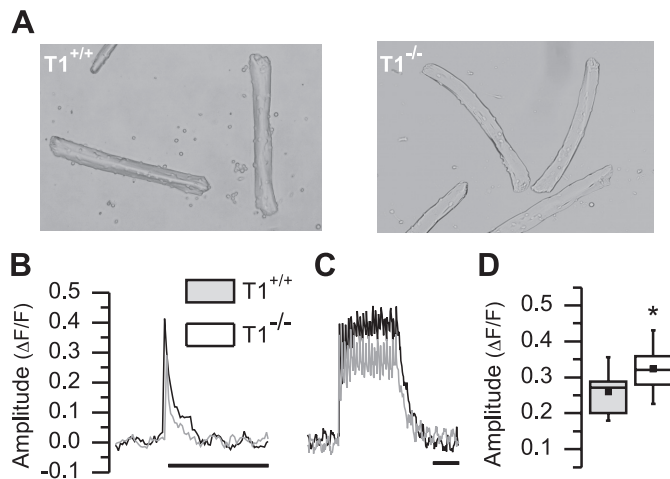


Fig. 4. Global voltage-dependent Ca<sup>2+</sup> signaling in single skeletal myofibers. A: representative photomicrograph of isolated flexor digitorum brevis (FDB) myofibers from adult *trkB.T1*<sup>+/+</sup> and *trkB.T1*<sup>-/-</sup> mice. B and C: Ca<sup>2+</sup> transients were measured using MagFluo-4AM (5 µM, 45 min) at 20–22°C; raw data traces (arbitrary y-axis) are displayed. The myofibers were activated by a single 500-µs square pulse (B) or trains of pulses (C, 100 Hz for 200 ms; black bar) delivered with two field electrodes placed ~2 mm apart across the myofiber. D: box plot representation of the peak amplitude (ΔF/F) of the fluorescent transient amplitude for *trkB.T1*<sup>+/+</sup> (gray box) or *trkB.T1*<sup>-/-</sup> mice (white box). Whiskers represent data points at the 5th and 95th percentiles, box extent and midline represent values at the 25th and 75th percentiles and median, and inset box is the mean value. n<sub>fibers</sub> = 8–12; n<sub>mice</sub> = 4/genotype; \*P = 0.03.

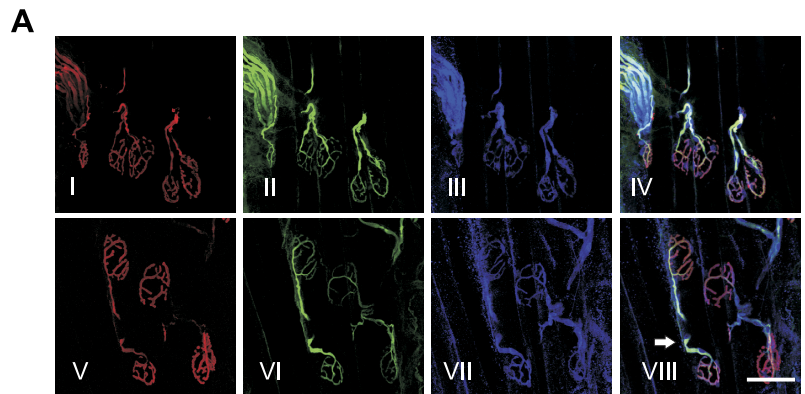
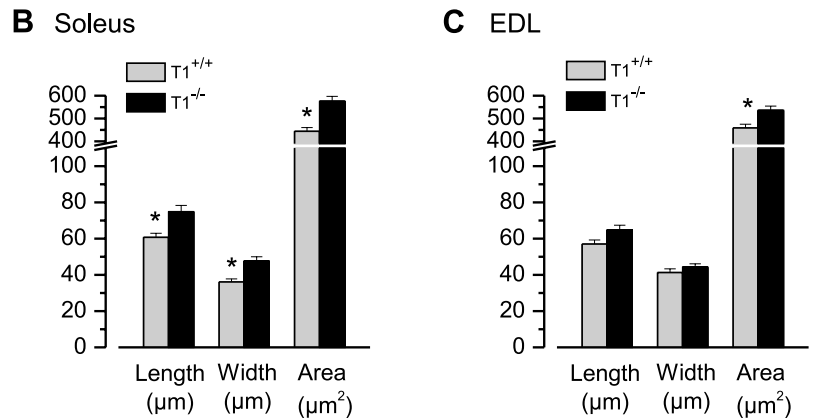


Fig. 5. Neuromuscular junction (NMJ) morphology. A: representative maximum plane projections of confocal stacks of individual NMJs from the EDL of an adult *trkB.T1*<sup>+/+</sup> (top) and *trkB.T1*<sup>-/-</sup> (bottom) animal. In these images, acetylcholine receptors (AChRs) are labeled with TRITC-conjugated  $\alpha$ -bungarotoxin (red), and exons and nerve terminals are labeled with antibodies to neurofilament and SV2 (green). Schwann cell area is labeled with antibodies to S-100 (blue). The overlay of labels in these images (IV, VIII) demonstrates the precise colocalization between the three cell types present at the NMJ and that the synaptic morphology between the *trkB.T1* control and deleted animals is similar. In VIII, the intramuscular nerve with myelinating Schwann cells is shown as indicated by the white arrow. Scale bar is 50  $\mu$ m. Image analysis (Metamorph) was used to examine length, width, and area of NMJs from soleus (B) and EDL (C) muscles from *trkB.T1*<sup>+/+</sup> (gray bars,  $n = 3$  mice) and *trkB.T1*<sup>-/-</sup> mice (black bars,  $n = 3$  mice). \* $P < 0.05$  by ANOVA.



( $1.65 \pm 0.11$  vs.  $4.36 \pm 0.46$ , respectively; Fig. 7B) following the exercise protocol.

#### Genetic Deletion of *trkB.T1* Reduces the Loss of Muscle-Specific Force Following Eccentric Injury

In recent studies, myogenic Akt signaling was activated by either pharmacological (4) or genetic approaches (7–8, 58) as an intervention for the muscle dysfunction seen in the *mdx* mouse, the murine model of Duchenne muscular dystrophy. In each study, an increase in activated Akt amplified the endogenous Akt-dependent compensatory mechanisms, which included increased expression of mRNA and proteins involved in cytoskeletal stability and membrane repair. These changes resulted in a protection from an acute eccentric injury paradigm in *mdx* muscle (8, 58) as well as in nondiseased (i.e., wild-type) muscle (7). Given these reports, and the enhancements in Akt-dependent signaling in the *trkB.T1*<sup>-/-</sup> muscle we identified, we evaluated the relative resistance to an acute eccentric injury in both *trkB.T1*<sup>+/+</sup> and *trkB.T1*<sup>-/-</sup> mice as well as examining the muscles for the select genes and proteins associated with cytoskeletal stability and membrane repair as recently described (8, 58).

Following methods established by our group, the knee of deeply anesthetized mice was stereotaxically immobilized while the foot was affixed to a custom footplate on a torque cell (28, 44, 62). After the determination of nerve-evoked peak isometric force of the dorsiflexor muscles (i.e., TA and EDL), single eccentric contractions were delivered once per minute for 20 min. One minute after the last contraction, peak isometric torque was again assessed. In Fig. 8A, we summarize the

percentage of isometric force loss following the eccentric injury. Here we find that *trkB.T1*<sup>-/-</sup> mice were significantly more resistant to eccentric injury than were *trkB.T1*<sup>+/+</sup> mice ( $50.03 \pm 2.72$  vs.  $40.87 \pm 1.55\%$  force drop in isometric force).

#### *trkB.T1* Depletion Results in Increased mRNA and Protein Expression of Cytoskeletal Stability and Membrane Repair Components

In the contralateral, uninjured TA muscle (i.e., the control limb) of the muscle injury experimental cohort ( $n = 5$  per genotype), as well as in an additional cohort not receiving experimental manipulation ( $n = 6$  per genotype), muscle was assayed for both gene expression and protein content of utrophin, desmin, and dysferlin, three proteins associated with Akt-dependent protection from eccentric injury (8, 58). To examine mRNA expression quantitatively, we sequenced TA muscle digital gene expression libraries from three wild-type and three *trkB.T1*<sup>-/-</sup> mice. We obtained an average of  $7.1 \times 10^6$  sequence reads per sample. Mean number of reads were obtained for each genotype and then we specifically examined the expression levels for desmin, dysferlin, and utrophin. In samples sequenced from muscle RNA extracted from the *trkB.T1*<sup>-/-</sup> mice, the expression of desmin was 135% greater than wild type while the expression of dysferlin was 395% greater than wild type. Utrophin expression was increased by 50%.

To confirm our gene expression findings, we examined protein expression in a set of protein lysates prepared from TA muscles from both genotypes (Fig. 8B). Western blot analysis

Table 3. Neuromuscular synaptic transmission of the soleus muscle from *trkB.T1*<sup>-/-</sup> (*n* = 4) and *trkB.T1*<sup>+/+</sup> (*n* = 4) mice

	Amplitude, mV	Frequency, Hz	<i>n</i>
<i>Mini-End-Plate Potential</i>			
T1 <sup>+/+</sup>	0.546 ± 0.027	1.141 ± 0.171	21
T1 <sup>-/-</sup>	0.545 ± 0.024	1.555 ± 0.173	23
	Amplitude, mV	Rise Time, ms	<i>n</i>
<i>End-Plate Potential</i>			
T1 <sup>+/+</sup>	24.700 ± 2.245	1.835 ± 0.142	23
T1 <sup>-/-</sup>	25.957 ± 2.196	1.952 ± 0.114	25
	No. of ACh Quanta/Pulse		<i>n</i>
<i>Average Quantal Content</i>			
T1 <sup>+/+</sup>	54.228 ± 12.438		19
T1 <sup>-/-</sup>	84.708 ± 18.950		20
	% of Initial		<i>n</i>
<i>Paired Pulse Facilitation</i>			
T1 <sup>+/+</sup>	0.959 ± 0.026		18
T1 <sup>-/-</sup>	0.955 ± 0.023		10

Values are population means ± SE for measurements of mini end-plate potential, end-plate potential, average quantal content, and paired pulse facilitation. No significant differences were seen between genotypes across these parameters. The *n* in the table represents no. of junctions tested in each condition from 4 mice of each genotype (*n* = 8).

of muscles from *trkB.T1*<sup>-/-</sup> mice revealed an increase in desmin and dysferlin compared with *trkB.T1*<sup>+/+</sup> muscles. We were not able to confirm the increase in utrophin expression, perhaps because of lack of sensitivity to detect this protein via Western blot analysis in wild-type muscle (58).

## DISCUSSION

Here we report that, consequent to the genetic deletion of *trkB.T1*, neuromuscular function and nerve-evoked muscle tension are significantly increased in vivo in *trkB.T1*<sup>-/-</sup> mice compared with *trkB.T1*<sup>+/+</sup> littermates. In vitro assays showed that, while this enhancement was independent of any improvement of synaptic function at the NMJ, an increase in muscle contractility and a gain in excitation-contraction (EC) coupling-evoked SR Ca<sup>2+</sup> release was identified in muscle from *trkB.T1*<sup>-/-</sup> mice. Consistent with *trkB.T1*'s role in cellular signaling in other cell types (21–22, 53, 71), we demonstrate that the deletion of *trkB.T1* increases neurotrophin-dependent activation of downstream signaling targets (e.g., Akt and p70/sk6) that likely contributed to these functional improvements identified in the *trkB.T1*<sup>-/-</sup>.

### Enhanced Neuromuscular Function in the *trkB.T1*<sup>-/-</sup> Is Associated With Postsynaptic Enhancements Within the Myofiber

Given that our initial results demonstrated enhanced nerve-evoked muscle force in vivo, we hypothesized that presynaptic mechanisms may be operant in this gain-of-function phenotype. Our rationale was based on either gain-of-function (45, 60) or loss-of-function (5, 25, 38) phenotypes previously seen

with modulation of *trkB.FL* or ligand (NT-4). In contrast to our hypothesis, we identified no difference in synaptic function in *trkB.T1*<sup>-/-</sup> muscle. We did, however, identify a modest but statistically significant increase in postsynaptic NMJ size and myofiber CSA in *trkB.T1*<sup>-/-</sup> myofibers.

Accumulating evidence exists for a postsynaptic axis for *trkB* modulation as recent studies report that neurotrophin ligands functionally affect peripheral tissues, including skeletal muscle (47, 60, 72, 74). The *trkB* ligand, BDNF, has been shown to preserve muscle fiber CSA after denervation (23, 51, 66). In addition, BDNF has been shown to regulate satellite cell function and muscle regeneration (17) after injury. Our current finding is the first to demonstrate that *trkB.T1* receptor expression has consequences at the level of the muscle cell.

In both the in vivo and the in vitro measures of contractile function, the results were normalized to either body weight/

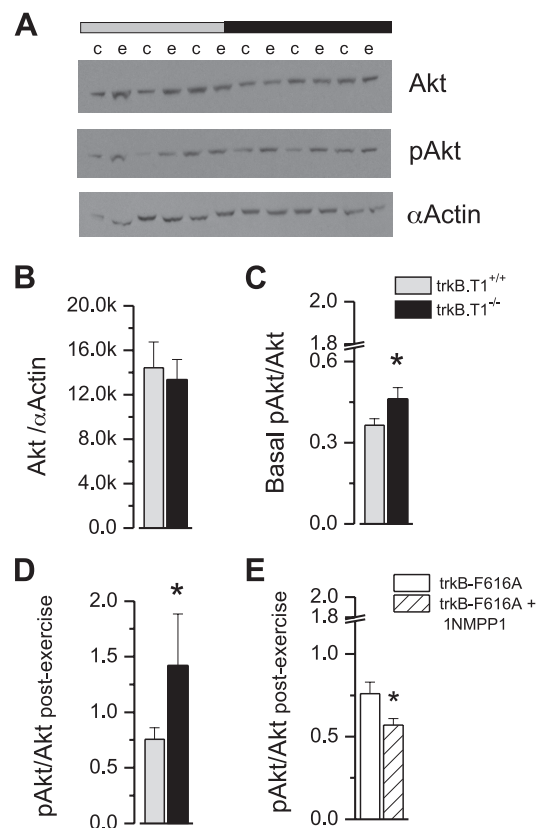


Fig. 6. Activity-dependent Akt (i.e., protein kinase B) is enhanced in *trkB.T1*<sup>-/-</sup> muscles. Equal volumes of tibialis anterior muscle homogenates were resolved on 4–12% SDS-PAGE, transferred to nitrocellulose membranes, and probed with primary antibodies against Akt, phosphorylated (p)Akt (Ser473). A: representative Western blot demonstrating Akt protein (top), pAkt (middle), and  $\alpha$ -actin (bottom) from *n* = 4 separate experiments (c, control; e, exercise). B: the content of Akt protein normalized to  $\alpha$ -actin was not different in muscles taken from *trkB.T1*<sup>+/+</sup> and *trkB.T1*<sup>-/-</sup> mice. C and D: the pAkt/Akt ratio from basal (C) and postexercise (D) conditions was significantly different in *trkB.T1*<sup>-/-</sup> compared with *trkB.T1*<sup>+/+</sup>; *n* = 4 separate experiments. \**P* < 0.05 by ANOVA. E: in similar response to the *trkB.T1*<sup>+/+</sup>, the *trkB.F616A* muscles displayed an approximate 0.75-fold increase of pAkt with stimulation, an effect that was approximately half that seen in the *trkB.T1*<sup>-/-</sup> (see D). Pretreatment with 1NMPP1, the small-molecule inhibitor of *trkB.FL* signaling, resulted in an ablation of the stimulation-induced pAkt when compared with the untreated control. Taken together, stimulation in *trkB.T1*<sup>-/-</sup> muscle resulted in an ~48% increase in pAkt over *trkB.T1*<sup>+/+</sup> while 1NMPP1 inhibition in the *trkB.F616A* mice resulted in a decrease in amount of pAkt in stimulated muscle by ~24%.

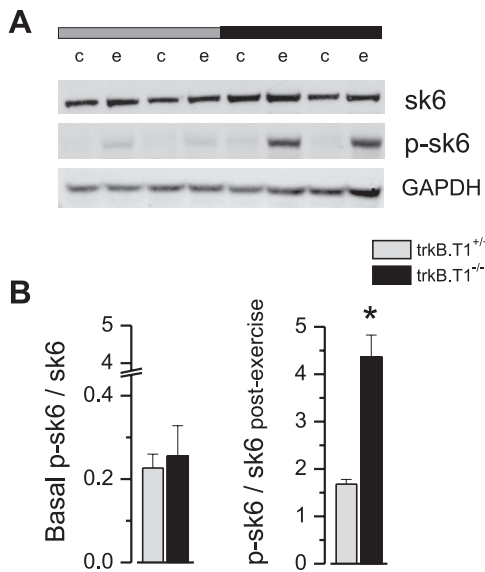


Fig. 7. Activity-dependent p70/S6 kinase (sk6) is enhanced in *trkB.T1*<sup>-/-</sup> muscles. Equal volumes of tibialis anterior muscle homogenate were resolved on 4–12% SDS-PAGE, transferred to nitrocellulose membranes, and probed with primary antibodies against sk6 and p-sk6. *A*: representative Western blot demonstrating sk6 protein (*top*), p-sk6 (*middle*), and GAPDH (*bottom*) from *n* = 4 separate experiments. No difference was seen in the relative amount of sk6 protein between genotypes compared with GAPDH as a loading control. *B*: nerve-evoked contractions induced a significant increase in phosphorylated sk6 over the basal condition in the *trkB.T1*<sup>-/-</sup> animals (4.36 ± 0.43-fold) when compared with the *trkB.T1*<sup>+/+</sup> (1.65 ± 0.11-fold). \**P* < 0.05.

muscle weight (in vivo) or cross-sectional area (in vitro). In each set of experiments, muscle force output was significantly higher in the *trkB.T1*<sup>-/-</sup> despite the body weights or muscle mass (TA, EDL, or soleus) being smaller in the *trkB.T1*<sup>-/-</sup> than the *trkB.T1*<sup>+/+</sup>. These results suggest that enhancement in muscle contractility explains the increased force production in the *trkB.T1*<sup>-/-</sup> mice.

An assay of global EC coupling processes revealed that myofibers from *trkB.T1*<sup>-/-</sup> mice exhibited a significant increase in the peak amplitude of the electrically elicited Ca<sup>2+</sup> transient compared with those from wild-type littermates. This increase in the magnitude of Ca<sup>2+</sup> transients occurred without a change in the rate of decay of the Ca<sup>2+</sup> transient. This suggests that, while Ca<sup>2+</sup> release from the SR was increased in mice lacking trkB.T1, the sequestration of Ca<sup>2+</sup> into intracellular stores was unchanged. In the context of EC coupling processes, an increase in the peak amplitude of Ca<sup>2+</sup> release is consistent with a greater peak Ca<sup>2+</sup> flux from the ryanodine receptor (RyR) Ca<sup>2+</sup> release channel in the SR.

Several reports support the notion that trkB-mediated signaling might affect RyR-dependent Ca<sup>2+</sup> release. For example, activation of trkB signaling via exogenous application of NT-4 enhances voltage-dependent RyR Ca<sup>2+</sup> release from intracellular stores in rat pyramidal neurons (36). Furthermore, an enhancement of force production secondary to ligand activation of trkB signaling was observed in airway smooth muscle, and this effect was dependent on Ca<sup>2+</sup> release from the SR (60). While we identified an enhancement in voltage-dependent SR Ca<sup>2+</sup> release in the *trkB.T1*<sup>-/-</sup> mice, we could not enhance this Ca<sup>2+</sup> release with acute (1 h) or chronic (24 h) exposure of wild-type or *trkB.T1*<sup>-/-</sup> myofibers to exogenous

NT-4 (see Supplemental Fig. S1). This result supports the findings of Mantilla et al. (45) as well as Zhan et al. (76), who have shown that acute neurotrophin application was not effective at modulating muscle specific contractility. Therefore, our results are most consistent with more chronic adaptive changes

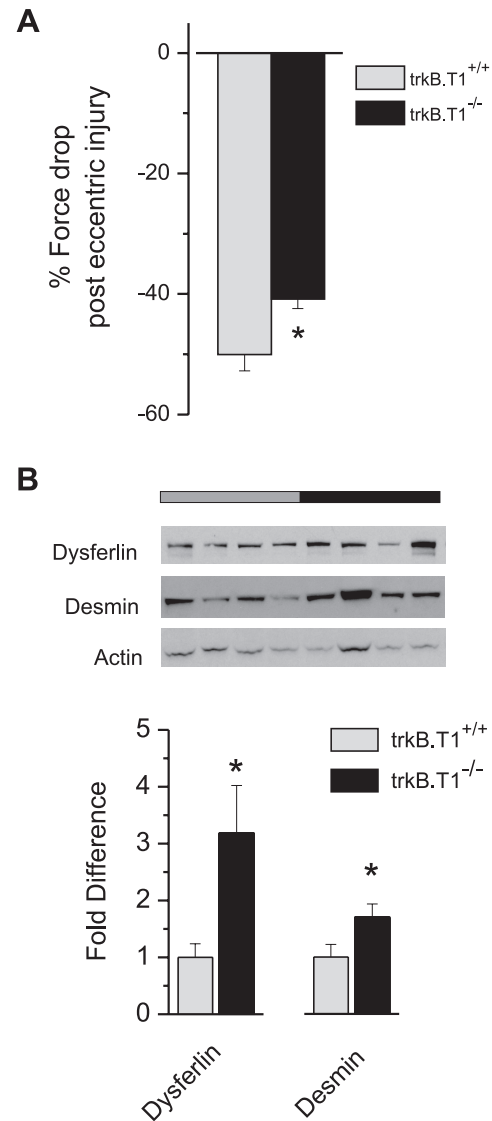


Fig. 8. *trkB.T1* deletion results in less susceptibility to injury. *A*: maximal torque was measured in the dorsiflexor muscles of *trkB.T1*<sup>+/+</sup> (*n* = 9) and *trkB.T1*<sup>-/-</sup> (*n* = 9) mice before and after the eccentric injury protocol (details are described in MATERIALS AND METHODS). Because we used a maximal tetanic contraction and we measured torque at a fixed ankle position, our measure of maximal torque ultimately reflects maximal muscle force. The deficit in isometric force generation following injury is presented as the % loss in isometric force after normalization to the preinjury level. While there was a substantial force deficit in both the *trkB.T1*<sup>+/+</sup> and the *trkB.T1*<sup>-/-</sup> animals, the *trkB.T1*<sup>-/-</sup> mice sustained significantly less injury compared with the *trkB.T1*<sup>+/+</sup> animals. \**P* = 0.008 by repeated measures ANOVA. *B*: clarified muscle homogenate was resolved on 4–12% SDS-PAGE, transferred to nitrocellulose membranes, and probed with primary antibodies against dysferlin (*top*) and desmin (*middle*). Blots were then stripped and reprobed with anti-actin primary antibodies to determine protein densities. The top set gray bar indicates *trkB.T1*<sup>+/+</sup>, and the black bar represents *trkB.T1*<sup>-/-</sup> samples. Bar graph demonstrates a significant increase in dysferlin and desmin protein in *trkB.T1*<sup>-/-</sup> muscles. *n* = 8 muscles/genotype; \**P* < 0.05 by ANOVA.

in EC coupling being responsible for the contractility phenotype in the *trkB.T1*<sup>-/-</sup> muscle fibers.

Several pieces of evidence argue against enhanced myofilament sensitivity as a significant contributor to the contractility. Here we found that MHC isoforms are similar across genotypes and that the shape of the normalized force vs. frequency relationship was identical, both supporting the idea that myofilament activations are similar. Indirect evidence comes from a recent study that used an inducible expression of myogenic Akt (7), which demonstrated an increase in muscle-specific force and EC coupling similar to that seen in the *trkB.T1*<sup>-/-</sup>. These investigators identified an increase in Ca<sup>2+</sup>-activated force production in skinned muscle segments that was fully explained by the resistance of the Akt-derived muscle segments to osmotic swelling post skinning (7), an experimental artifact that alters the actin-myosin interaction and lowers force production. Interestingly, we identified an overexpression of cytoskeletal proteins (e.g., desmin and dysferlin) in the *trkB.T1*<sup>-/-</sup> that are known to be overexpressed with Akt activation in skeletal muscle (58) and could thus serve to protect cells from mechanical stresses such as osmotic swelling as well as eccentric muscle damage (see below).

In our final set of experiments, we demonstrated that the deletion of *trkB.T1* proffered protection against the loss of maximal isometric force following an acute eccentric contraction injury protocol. Across two sets of experiments (9 animals per genotype), we report a significant ~10% ( $P < 0.05$ ) decrease in isometric torque loss in the *trkB.T1*<sup>-/-</sup> mice following eccentric injury. The acute loss in muscle force with eccentric injury can be the result of cytoskeletal damage and/or membrane disruption (44, 62), and our results suggest that the *trkB.T1*<sup>-/-</sup> mice are likely protected in one or both areas. In this regard, we find that *trkB.T1* mice have an increase in the mRNA and the protein content of both dysferlin, a protein integral to the membrane repair process (3, 39, 62), and desmin, a cytoskeletal protein shown to provide stability to the contractile apparatus and cytoskeletal-sarcolemmal interface (3, 39, 42, 62). In fact, recent work used drastic overexpression of activated Akt in the *mdx* mouse, achieved a increase in dysferlin and desmin, and demonstrated a decrease isometric torque loss by ~20% following eccentric injury (8). Given that we show a 10% protection of force drop in the nondiseased *trkB.T1*<sup>-/-</sup> muscles, we believe that these results are not only statistically significant but physiologically significant.

### *The trkB Loci As a Target for Improving Muscle Function*

Within the skeletal myofiber, neurotrophin ligand (NT-4/5/BDNF) is released by muscle fibers in an activity-dependent manner (5, 14, 45, 47, 59). Furthermore, it is well established that skeletal muscle has both the full length and truncated isoforms of trkB (25, 27, 47, 55, 59). Given the presence of this ligand and receptor system in muscle, our results are consistent with the parsimonious model in which *trkB.T1* acts in a dominant negative manner to inhibit trkB.FL signaling (24, 25). In this model, the presence of *trkB.T1* would act to limit homodimerization of trkB.FL and thus limit trkB-dependent signaling to downstream targets. In contrast, the muscle from *trkB.T1*<sup>-/-</sup> mice would be predicted to present with an increased gain in activity-dependent trkB signaling to down-

stream targets given the lack of dominant negative inhibition, a result we demonstrate here.

In our current study, we have evidence that the deletion of *trkB.T1* increases neurotrophin-dependent activation of downstream signaling to Akt and p70/sk6 and it is likely that this gain in trkB-dependent signaling played a role in the phenotypes identified. Indirect support for this signaling axis as a contributor *trkB.T1*<sup>-/-</sup> phenotype comes from recent studies in which constitutively activated Akt (58) or short-term inducible activated Akt (7) induced an increase in in vivo muscle contractility that was accompanied by increased in vitro force production, no change in muscle fiber type, increased EC coupling-dependent SR Ca<sup>2+</sup> release as well as resistance to eccentric injury, all findings we demonstrate in the *trkB.T1*<sup>-/-</sup>.

While this simplistic model conceptually accounts for our findings, we acknowledge that other studies have suggested unique signaling roles for *trkB.T1*, for example, by modulating Ca<sup>2+</sup> signaling mechanisms (63). Here we report that EC coupling-dependent SR Ca<sup>2+</sup> release is enhanced in *trkB.T1*<sup>-/-</sup> muscle fibers. While there is evidence that enhanced Akt-dependent signaling can lead to increases in muscle contractility (16, 46, 57, 64), we cannot rule out an alternative possibility that, secondary to *trkB.T1*<sup>-/-</sup> deletion, mice have an increase in EC coupling-dependent Ca<sup>2+</sup> release that would lead to increased force production, increased excitation/transcriptional coupling (43, 52, 65), and an increase in Akt activation. Indeed, there is evidence that neurotrophin activation could act by increasing membrane excitability and Ca<sup>2+</sup> release which would be a chronic activator of Akt at rest as well as during activity; both we identified in the *trkB.T1*<sup>-/-</sup> (34, 63, 77).

Across all cell types that express trkB.T1, the role of this receptor in cell function and detail of its signaling are still not fully understood. While future investigations directed at revealing the mechanistic details of trkB.T1 signaling are needed, our novel finding of enhanced neuromuscular performance with the genetic deletion of *trkB.T1* as well the reduction in eccentric injury in the *trkB.T1*<sup>-/-</sup> mice supports the trkB loci as a target for intervention across diseases characterized by deficits in muscle contractility.

### ACKNOWLEDGMENTS

We thank Kimberly Valentino, Katie Zuchowski, and Marion O. Scott for technical assistance.

### GRANTS

This work was supported by grants from the National Institutes of Health to C. W. Ward (AR002177, AR053318, and RC2 NR011968), to S. G. Dorsey (NR009672 and NR011968), to R. M. Wyatt (NS047777), to R. Lovering (K01AR053235 and 1R01AR059179), and to R. Balice-Gordon (NS046490), and by intramural support from the National Cancer Institute Center for Cancer Research to C. Barrick and L. J. Tallon and intramural support from the National Institute of Drug Abuse to B. K. Harvey.

### DISCLOSURES

No conflicts of interest, financial or otherwise, are declared by the author(s).

### AUTHOR CONTRIBUTIONS

Author contributions: S.G.D., R.L., L.J.T., A.P., R.T., C.Z., K.S., C.F.-L., R.J.B.-G., L.T., and C.W.W. conception and design of research; S.G.D., R.L., C.L.R., C.C.L., X.L., L.J.T., L.D.S., A.P., S.O., N.S., K.M.J., C.B., G.F., J.B., K.V., R.T., B.K.H., R.M.W., E.V.-P., R.J.B.-G., and C.W.W. performed experiments; S.G.D., R.L., K.V., R.T., B.K.H., C.F.-L., R.J.B.-G., L.T., and

C.W.W. interpreted results of experiments; S.G.D., R.L., C.L.R., R.J.B.-G., and C.W.W. edited and revised manuscript; S.G.D., R.L., C.L.R., C.C.L., X.L., L.J.T., L.D.S., A.P., S.O., N.S., K.M.J., C.B., G.F., J.B., K.V., R.T., B.K.H., R.M.W., E.V.-P., C.Z., K.S., C.F.-L., R.J.B.-G., L.T., and C.W.W. approved final version of manuscript; R.L., C.C.L., X.L., L.J.T., K.V., R.T., B.K.H., R.M.W., E.V.-P., R.J.B.-G., L.T., and C.W.W. analyzed data; C.W.W. prepared figures; C.W.W. drafted manuscript.

## REFERENCES

- Abramow-Newerly W, Lipina T, Abramow-Newerly M, Kim D, Becharod AR, Xie G, Clapcote SJ, Roder JC. Methods to rapidly and accurately screen a large number of ENU mutagenized mice for abnormal motor phenotypes. *Amyotroph Lateral Scler* 7: 112–118, 2006.
- Balice-Gordon RJ, Breedlove SM, Bernstein S, Lichtman JW. Neuromuscular junction shrink and expand as muscle fiber size is manipulated: in vivo observations in the androgen-sensitive bulbocavernosus muscle of mice. *J Neurosci* 10: 2660–2671, 1990.
- Bansal D, Miyake K, Vogel SS, Groh S, Chen CC, Williamson R, McNeil PL, Campbell KP. Defective membrane repair in dysferlin-deficient muscular dystrophy. *Nature* 423: 168–172, 2003.
- Barton ER, Morris L, Musaro A, Rosenthal N, Sweeney HL. Muscle-specific expression of insulin-like growth factor I counters muscle decline in *mdx* mice. *J Cell Biol* 157: 137–148, 2002.
- Belluardo N, Westerblad H, Mudo G, Casabona A, Bruton J, Caniglia G, Pastoris O, Grassi F, Ibanez CF. Neuromuscular junction disassembly and muscle fatigue in mice lacking neurotrophin-4. *Mol Cell Neurosci* 18: 56–67, 2001.
- Berchtold MW, Brinkmeier H, Muntener M. Calcium ion in skeletal muscle: its crucial role for muscle function, plasticity, and disease. *Physiol Rev* 80: 1215–1265, 2000.
- Blaauw B, Canato M, Agatea L, Toniolo L, Mammucari C, Masiero E, Abraham R, Sandri M, Schiaffino S, Reggiani C. Inducible activation of Akt increases skeletal muscle mass and force without satellite cell activation. *FASEB J* 23: 3896–3905, 2009.
- Blaauw B, Mammucari C, Toniolo L, Agatea L, Abraham R, Sandri M, Reggiani C, Schiaffino S. Akt activation prevents the force drop induced by eccentric contractions in dystrophin-deficient skeletal muscle. *Hum Mol Genet* 17: 3686–3696, 2008.
- Brown LD, Rodney GG, Hernández-Ochoa E, Ward CW, Schneider MF. Ca<sup>2+</sup> sparks and T tubule reorganization in dedifferentiating adult mouse skeletal muscle fibers. *Am J Physiol Cell Physiol* 292: C1156–C1166, 2007.
- Burkholder TJ, Lieber RL. Sarcomere number adaptation after retinaculum transection in adult mice. *J Exp Biol* 201: 309–316, 1998.
- Capote J, Bolanos P, Schuhmeier RP, Melzer W, Caputo C. Calcium transients in developing mouse skeletal muscle fibres. *J Physiol* 564: 451–464, 2005.
- Chao MV. Neurotrophin and their receptors: a convergence point for many signalling pathways. *Nat Rev Neurosci* 4: 299–309, 2003.
- Chen X, Ye H, Kuruvilla R, Ramanan N, Scangos KW, Zhang C, Johnson NM, England PM, Shokat KM, Ginty DD. A chemical-genetic approach to studying neurotrophin signaling. *Neuron* 46: 13–21, 2005.
- Chevrel G, Hohlfeld R, Sendtner M. The role of neurotrophins in muscle under physiological and pathological conditions. *Muscle Nerve* 33: 462–476, 2006.
- Chun LG, Ward CW, Schneider MF. Ca<sup>2+</sup> sparks are initiated by Ca<sup>2+</sup> entry in embryonic mouse skeletal muscle and decrease in frequency postnatally. *Am J Physiol Cell Physiol* 285: C686–C697, 2003.
- Cittadini A, Monti MG, Iaccarino G, Di Rella F, Tschlich PN, Di Gianni A, Stromer H, Sorriento D, Peschle C, Trimarco B, Sacca L, Condorelli G. Adenoviral gene transfer of Akt enhances myocardial contractility and intracellular calcium handling. *Gene Ther* 13: 8–19, 2006.
- Clow C, Jasmin BJ. Brain-derived neurotrophic factor regulates satellite cell differentiation and skeletal muscle regeneration. *Mol Biol Cell* 21: 2182–2190, 2010.
- Cohn RD, van Erp C, Habashi JP, Soleimani AA, Klein EC, Lisi MT, Gamradt M, Ap Rhys CM, Holm TM, Loeys BL, Ramirez F, Judge DP, Ward CW, Dietz HC. Angiotensin II type 1 receptor blockade attenuates TGF-beta-induced failure of muscle regeneration in multiple myopathic states. *Nat Med* 13: 204–210, 2007.
- Del Castillo J, Katz B. Quantal components of the end-plate potential. *J Physiol* 124: 560–573, 1954.
- Del Castillo J, Katz B. Statistical factors involved in neuromuscular facilitation and depression. *J Physiol* 124: 574–585, 1954.
- Dorsey SG, Bambrick LL, Balice-Gordon RJ, Krueger BK. Failure of brain-derived neurotrophic factor-dependent neuron survival in mouse trisomy 16. *J Neurosci* 22: 2571–2578, 2002.
- Dorsey SG, Renn CL, Carim-Todd L, Barrick CA, Bambrick L, Krueger BK, Ward CW, Tessarollo L. In vivo restoration of physiological levels of truncated TrkB. T1 receptor rescues neuronal cell death in a trisomic mouse model. *Neuron* 51: 21–28, 2006.
- Dupont-Versteegden EE, Houle JD, Dennis RA, Zhang J, Knox M, Wagoner G, Peterson CA. Exercise-induced gene expression in soleus muscle is dependent on time after spinal cord injury in rats. *Muscle Nerve* 29: 73–81, 2004.
- Eide FF, Vining ER, Eide BL, Zang K, Wang XY, Reichardt LF. Naturally occurring truncated trkB receptors have dominant inhibitory effects on brain-derived neurotrophic factor signaling. *J Neurosci* 16: 3123–3129, 1996.
- Gonzalez M, Ruggiero FP, Chang Q, Shi YJ, Rich MM, Kraner S, Balice-Gordon RJ. Disruption of Trkb-mediated signaling induces disassembly of postsynaptic receptor clusters at neuromuscular junction. *Neuron* 24: 567–583, 1999.
- Griesbeck O, Parsadanian AS, Sendtner M, Thoenen H. Expression of neurotrophin in skeletal muscle: quantitative comparison and significance for motoneuron survival and maintenance of function. *J Neurosci Res* 42: 21–33, 1995.
- Hammond JW, Hinton RY, Curl LA, Muriel JM, Lovering RM. Use of autologous platelet-rich plasma to treat muscle strain injuries. *Am J Sports Med* 37: 1135–1142, 2009.
- Holtmann B, Wiese S, Samsam M, Grohmann K, Pennica D, Martini R, Sendtner M. Triple knock-out of CNTF, LIF, and CT-1 defines cooperative and distinct roles of these neurotrophic factors for motoneuron maintenance and function. *J Neurosci* 25: 1778–1787, 2005.
- Huang EJ, Reichardt LF. Trk receptors: roles in neuronal signal transduction. *Annu Rev Biochem* 72: 609–642, 2003.
- Ingalls CP, Warren GL, Williams JH, Ward CW, Armstrong RB. E-C coupling failure in mouse EDL muscle after in vivo eccentric contractions. *J Appl Physiol* 85: 58–67, 1998.
- Ingalls CP, Warren GL, Zhang JZ, Hamilton SL, Armstrong RB. Dihydropyridine and ryanodine receptor binding after eccentric contractions in mouse skeletal muscle. *J Appl Physiol* 96: 1619–1625, 2004.
- Ingalls CP, Wenke JC, Nofal T, Armstrong RB. Adaptation to lengthening contraction-induced injury in mouse muscle. *J Appl Physiol* 97: 1067–1076, 2004.
- Kafitz KW, Rose CR, Thoenen H, Konnerth A. Neurotrophin-evoked rapid excitation through TrkB receptors. *Nature* 401: 918–921, 1999.
- Kaplan DR, Miller FD. Neurotrophin signal transduction in the nervous system. *Curr Opin Neurobiol* 10: 381–391, 2000.
- Kato N, Tanaka T, Yamamoto K, Isomura Y. Enhancement of activity-dependent calcium increase by neurotrophin-4 in visual cortex pyramidal neurons. *Brain Res* 832: 179–183, 1999.
- Kopp DM, Perkel DJ, Balice-Gordon RJ. Disparity in neurotransmitter release probability among competing inputs during neuromuscular synapse elimination. *J Neurosci* 20: 8771–8779, 2000. Kopp DM, Perkel DJ, Balice-Gordon RJ.
- Kulakowski SA, Parker SD, Personius KE. Reduced TrkB expression results in precocious age-like changes in neuromuscular structure, neurotransmission, and muscle function. *J Appl Physiol* 111: 844–852, 2011.
- Lennon NJ, Kho A, Bacskai BJ, Perlmutter SL, Hyman BT, Brown RH Jr. Dysferlin interacts with annexins A1 and A2 and mediates sarcolemmal wound-healing. *J Biol Chem* 278: 50466–50473, 2003.
- Li HS, Xu XZ, Montell C. Activation of a TRPC3-dependent cation current through the neurotrophin BDNF. *Neuron* 24: 261–273, 1999.
- Li Z, Oh DY, Nakamura K, Thiele CJ. Perifosine-induced inhibition of akt attenuates brain-derived neurotrophic factor/TrkB-induced chemoresistance in neuroblastoma in vivo. *Cancer*. In press.
- Lieber RL, Shah S, Friden J. Cytoskeletal disruption after eccentric contraction-induced muscle injury. *Clin Orthop Relat Res Suppl*: S90–S99, 2002.
- Liu Y, Shen T, Randall WR, Schneider MF. Signaling pathways in activity-dependent fiber type plasticity in adult skeletal muscle. *J Muscle Res Cell Motil* 26: 13–21, 2005.
- Lovering RM, Roche JA, Bloch RJ, De Deyne PG. Recovery of function in skeletal muscle following 2 different contraction-induced injuries. *Arch Phys Med Rehabil* 88: 617–625, 2007.

45. Mantilla CB, Zhan WZ, Sieck GC. Neurotrophins improve neuromuscular transmission in the adult rat diaphragm. *Muscle Nerve* 29: 381–386, 2004.
46. Mao K, Kobayashi S, Jaffer ZM, Huang Y, Volden P, Chernoff J, Liang Q. Regulation of Akt/PKB activity by P21-activated kinase in cardiomyocytes. *J Mol Cell Cardiol* 44: 429–434, 2008.
47. Matthews VB, Astrom MB, Chan MH, Bruce CR, Krabbe KS, Prelovsek O, Akerstrom T, Yfanti C, Broholm C, Mortensen OH, Penkova M, Hojman P, Zankari A, Watt MJ, Bruunsgaard H, Pedersen BK, Febbraio MA. Brain-derived neurotrophic factor is produced by skeletal muscle cells in response to contraction and enhances fat oxidation via activation of AMP-activated protein kinase. *Diabetologia* 52: 1409–1418, 2009.
48. McLachlan EM, Martin AR. Non-linear summation of end-plate potentials in the frog and mouse. *J Physiol* 311: 307–324, 1981.
49. Mendez J, Keys A. Density and composition of mammalian muscle. *Metabolism* 9: 184–188, 1960.
50. Middlemas DS, Lindberg RA, Hunter T. trkB, a neural receptor protein-tyrosine kinase: evidence for a full-length and two truncated receptors. *Mol Cell Biol* 11: 143–153, 1991.
51. Mousavi K, Parry DJ, Jasmin BJ. BDNF rescues myosin heavy chain IIB muscle fibers after neonatal nerve injury. *Am J Physiol Cell Physiol* 287: C22–C29, 2004.
52. Mu X, Brown LD, Liu Y, Schneider MF. Roles of the calcineurin and CaMK signaling pathways in fast-to-slow fiber type transformation of cultured adult mouse skeletal muscle fibers. *Physiol Genomics* 30: 300–312, 2007.
53. Nguyen N, Lee SB, Lee YS, Lee KH, Ahn JY. Neuroprotection by NGF and BDNF against neurotoxin-exerted apoptotic death in neural stem cells are mediated through Trk receptors, activating PI3-kinase and MAPK pathways. *Neurochem Res* 34: 942–951, 2009.
54. O'Malley JP, Waran MT, Balice-Gordon RJ. In vivo observations of terminal Schwann cells at normal, denervated, and reinnervated mouse neuromuscular junction. *J Neurobiol* 38: 270–286, 1999.
55. Ogborn DI, Gardiner PF. Effects of exercise and muscle type on BDNF, NT-4/5, and TrkB expression in skeletal muscle. *Muscle Nerve* 41: 385–391, 2010.
56. Payne ET, Yasuda N, Bourgeois JM, Devries MC, Rodriguez MC, Yousuf J, Tarnopolsky MA. Nutritional therapy improves function and complements corticosteroid intervention in mdx mice. *Muscle Nerve* 33: 66–77, 2006.
57. Peter AK, Crosbie RH. Hypertrophic response of Duchenne and limb-girdle muscular dystrophies is associated with activation of Akt pathway. *Exp Cell Res* 312: 2580–2591, 2006.
58. Peter AK, Ko CY, Kim MH, Hsu N, Ouchi N, Rhee S, Izumiya Y, Zeng L, Walsh K, Crosbie RH. Myogenic Akt signaling upregulates the utrophin-glycoprotein complex and promotes sarcolemma stability in muscular dystrophy. *Hum Mol Genet* 18: 318–327, 2009.
59. Pitts EV, Potluri S, Hess DM, Balice-Gordon RJ. Neurotrophin and Trk-mediated signaling in the neuromuscular system. *Int Anesthesiol Clin* 44: 21–76, 2006.
60. Prakash YS, Iyanoye A, Ay B, Mantilla CB, Pabelick CM. Neurotrophin effects on intracellular Ca<sup>2+</sup> and force in airway smooth muscle. *Am J Physiol Lung Cell Mol Physiol* 291: L447–L456, 2006.
61. Reichardt LF. Neurotrophin-regulated signalling pathways. *Philos Trans R Soc Lond B Biol Sci* 361: 1545–1564, 2006.
62. Roche JA, Lovering RM, Bloch RJ. Impaired recovery of dysferlin-null skeletal muscle after contraction-induced injury in vivo. *Neuroreport* 19: 1579–1584, 2008.
63. Rose CR, Blum R, Pichler B, Lepier A, Kafitz KW, Konnerth A. Truncated TrkB-T1 mediates neurotrophin-evoked calcium signalling in glia cells. *Nature* 426: 74–78, 2003.
64. Schiekofe S, Shiojima I, Sato K, Galasso G, Oshima Y, Walsh K. Microarray analysis of Akt1 activation in transgenic mouse hearts reveals expression profiles associated with compensatory hypertrophy and failure. *Physiol Genomics* 27: 156–170, 2006.
65. Shen T, Liu Y, Randall WR, Schneider MF. Parallel mechanisms for resting nucleocytoplasmic shuttling and activity dependent translocation provide dual control of transcriptional regulators HDAC and NFAT in skeletal muscle fiber type plasticity. *J Muscle Res Cell Motil* 27: 405–411, 2006.
66. Simon M, Porter R, Brown R, Coulton GR, Terenghi G. Effect of NT-4 and BDNF delivery to damaged sciatic nerves on phenotypic recovery of fast and slow muscles fibres. *Eur J Neurosci* 18: 2460–2466, 2003.
67. Stack EC, Kubilus JK, Smith K, Cormier K, Del Signore SJ, Guelin E, Ryu H, Hersch SM, Ferrante RJ. Chronology of behavioral symptoms and neuropathological sequela in R6/2 Huntington's disease transgenic mice. *J Comp Neurol* 490: 354–370, 2005.
68. Talmadge RJ, Otis JS, Rittler MR, Garcia ND, Spencer SR, Lees SJ, Naya FJ. Calcineurin activation influences muscle phenotype in a muscle-specific fashion. *BMC Cell Biol* 5: 28, 2004.
69. Talmadge RJ, Roy RR. Electrophoretic separation of rat skeletal muscle myosin heavy-chain isoforms. *J Appl Physiol* 75: 2337–2340, 1993.
70. Talmadge RJ, Roy RR, Edgerton VR. Persistence of hybrid fibers in rat soleus after spinal cord transection. *Anat Rec* 255: 188–201, 1999.
71. Troca-Marin JA, Alves-Sampaio A, Montesinos ML. An increase in basal BDNF provokes hyperactivation of the Akt-mammalian target of rapamycin pathway and deregulation of local dendritic translation in a mouse model of Down's syndrome. *J Neurosci* 31: 9445–9455, 2011.
72. Wiedemann FR, Siemen D, Mawrin C, Horn TF, Dietzmann K. The neurotrophin receptor TrkB is colocalized to mitochondrial membranes. *Int J Biochem Cell Biol* 38: 610–620, 2006.
73. Williams JH, Ward CW, Spangenburg EE, Nelson RM. Functional aspects of skeletal muscle contractile apparatus and sarcoplasmic reticulum after fatigue. *J Appl Physiol* 85: 619–626, 1998.
74. Yamanaka M, Tsuchida A, Nakagawa T, Nonomura T, Ono-Kishino M, Sugaru E, Noguchi H, Taiji M. Brain-derived neurotrophic factor enhances glucose utilization in peripheral tissues of diabetic mice. *Diabetes Obes Metab* 9: 59–64, 2007.
75. Yin X, Kidd GJ, Pioro EP, McDonough J, Dutta R, Feltri ML, Wrabetz L, Messing A, Wyatt RM, Balice-Gordon RJ, Trapp BD. Dysmyelinated lower motor neurons retract and regenerate dysfunctional synaptic terminals. *J Neurosci* 24: 3890–3898, 2004.
76. Zhan WZ, Mantilla CB, Sieck GC. Regulation of neuromuscular transmission by neurotrophins. *Sheng Li Xue Bao* 55: 617–624, 2003.
77. Zheng F, Soellner D, Nunez J, Wang H. The basal level of intracellular calcium gates the activation of phosphoinositide 3-kinase-Akt signaling by brain-derived neurotrophic factor in cortical neurons. *J Neurochem* 106: 1259–1274, 2008.